Technical Sciences4
Academy of Romania
www.jesi.astr.ro

Journal of Engineering Sciences and Innovation
Volume 9, Issue 2 / 2024, pp. 149 - 168

D. Environmental Engineering and Energy

Received ***21 Juny 2023*** *Accepted* ***14 June 2024***
Received in revised form ***14 February 2024***

Best operation strategies for piezoelectric vibration energy harvesters. III. Application to controllable inductance and capacitive loads

VIOREL BĂDESCU[*]

Candida Oancea Institute, National University for Science and Technology Politehnica Bucureşti, Spl. Independentei 313, Bucharest 060042, Romania

Abstract. A general scheme of controlling the operation of piezoelectric vibration energy harvesters is proposed. When the load consists of a resistor and a controllable inductance, the maximum harvested energy depends on the value of the load resistance. For resistances much smaller than the resonance value most energy is harvested in the first cycle while the next cycles contribute a small amount of energy. For large number of cycles, the inductance may be used as a control when the load resistance is smaller than the resonance value provided its interval of variation is large enough. When the resistance equals the resonance value it is not recommended to use the inductance as a control. When the load consists of a controllable capacitor, the optimal capacitance value is constant and equals the smallest allowed value. The capacitance should be large enough to store the energy needed by the user during a limited number of cycles of the vibratory energy sources. General conclusions: (i) he maximum harvesting performance is obtained when the control parameters are constant or have a bang-bang-type time evolution; (ii) the number of cycles used for optimization is an important design parameter, especially in case of storing energy in capacitors; (iii) the most suitable applications are those which may be powered by using the energy harvested from a single cycle.

Keywords: piezoelectric energy harvester; direct optimal control; controllable inductance. capacitance load.

1. Introduction

Several electric loads have been considered separately for vibration energy harvesting systems. The theory has been proposed in part I of the paper [1]. Inductors are used in different schemes of energy harvesting systems such as the synchronous electric charge extraction and the synchronized switch harvesting on

[*]Correspondence address: badescu@theta.termo.pub.ro

inductor [2]. One of the schemes considered in this paper includes an inductor. The novelty is that here we are using the inductor as a control. Also, here we focus on piezoelectric energy harvesters whose electrical load consists of a capacitor whose operation is optimally controlled. The objective is to maximize the energy extracted during each period. The optimization is performed for a large number of cycles as well as on a single cycle and when each of the two cases is useful in application is discussed.

2. Ferroelectric materials

Several ferroelectric materials have good piezoelectric properties. The material PZT-5H is considered here. Comparisons with results obtained for other material (PZT-5A) are shown in the Electronic Supplementary Material (ESM) of paper [3]. Further information about the system may be found in [4] including design details which are shortly presented in Table 1. These values are used in this work. Exceptions are clearly specified when needed.

Table 1. Main characteristics of the system treated here.

Piezoelectric material properties (PZT-5H)	
Stiffness coefficient (in short circuit conditions), c_{33}^{E}	$48.3\cdot10^{9}\ N/m^{2}$
Piezoelectric constant, e_{33}	$28.64\ C/m^{2}$
Permittivity of the piezoelectric element, ε_{33}^{S}	$1.317\cdot10^{-8}\ F/m$
Design quantities	
Cross sectional surface area through the piezoelectric element, A_p	$10^{-4}\ m^{2}$
Thickness of un-deformed piezoelectric element, t_p	$10^{-2}\ m$
Proof mass, M	$0.01\ kg$
Mass of piezoelectric element, m_p	$0.0075\ kg$
Mechanical damping ratio, ζ_m	0.05
Characteristics of the vibratory energy source (the base excitation)	
Frequency, $f=\dfrac{\omega}{2\pi}$	$120\ Hz$
Magnitude of acceleration, a	$1.276\ m/s^{2}$

3. Usage of a load inductance as a control

Inductance effects are usually neglected during optimization of energy harvesting systems operation [5].Two of the three energy harvesting systems considered in [2] include inductors. The synchronized switch harvesting on inductor (SSHI) system has the inductor placed near the transducer (Fig. 3 of [2]) while the synchronous electric charge extraction (SECE) system has the inductor placed after the

rectifying bridge (Fig. 2 of [2]). The energy harvesting system under harmonic excitation treated in [4] is adopted in [6], as we did here. In addition, an inductor placed in parallel or series with the resistance load is considered in [6] following previous studies which focused on the analysis of the damping resulting from energy harvesting. It has been shown that these systems provide better performance than purely resistive loads.

Figure 1 of paper [3] consists of two subfigures. The scheme in Fig. 1b is similar with that of Fig. 1a except the load consists of a resistor of resistance R_l and an inductor of controllable inductance L_l. The harvesting system presented in Fig. 1b of [3] has the inductor placed in series the resistance load. The inductors in [2] and [6] have fixed inductance while here we assume controllable inductance. The analysis presented in [6] consists of usual constrained steady-state optimization while here we performed an optimal control analysis.

By definition, the current i_h trough the load equals the time variation of its electrical charge:

$$i_h \equiv \dot{q}_h \tag{1}$$

Usage of Eqs. (2), (3) and (4) of paper [3] and Eq. (1) yields:

$$\dot{q}_t = \frac{v_t}{R_{hp}} + \dot{q}_h \tag{2}$$

Usage of Kirchoff's law for circuits gives:

$$v_t = \dot{q}_h R_{hs} + L_l \ddot{q}_h + \dot{q}_h R_l \tag{3}$$

The first and third terms in the r.h.s. member of Eq. (3) are the voltage drops across the resistances R_{hs} and R_l, respectively, while the second term is the voltage generated across the inductor due to the time variation of the current i_h. Usage of Eq. (7) of paper [3] and Eq. (2) yield:

$$\dot{q}_t = \frac{q_t + \theta z}{C_p R_{hp}} + \dot{q}_h \tag{4}$$

while Eq. (3) may be re-written as:

$$\ddot{q}_h = \frac{1}{L_l}\left[-\frac{q_t + \theta z}{C_p} - \left(R_{hs} + R_l\right)\dot{q}_h \right] \tag{5}$$

Equations (6) of pager [3], and Eqs. (4) and (5) constitute a system of three equations with three unknown, i.e. z, q_t and q_h.

Equation (6) of paper [3] and Eq. (4) are solved by using the initial conditions Eqs. (8) and (9) of paper [3], respectively, while the initial condition for Eq. (5) is:

$$q_h\left(\tau = 0\right) = 0 \tag{6}$$

The electric energy $E_{l,T}$ dissipated as heat on the load resistor during the time interval T is:

$$E_{l,T} = \int_0^T R_l i_h^2 d\tau = \int_0^T R_l \dot{q}_h^2 d\tau \qquad (7, \text{a,b})$$

Equation (1) has been used in Eq. (7b). The objective is to maximize the electric energy $E_{l,T}$ by using a time variable inductance L_l, which is used as a control.
Transformation of the Bolza problem into a Mayer problem implies first to define the new dependent variable E_l by using the equation:

$$\frac{dE_l}{d\tau} = R_l \dot{q}_h^2 \qquad (8)$$

The initial condition Eq. (12) of paper [3] and the objective Eq. (13) of paper [3] apply here, too.

Table 2 shows the dimensionless notation, the coefficients and the equations for a system where the load consists of a resistor and a controllable inductance.

3.1. Results

Here we make the assumption that the vibratory movement consists of similar cycles and a number of ten cycles is analyzed. In terms of the dimensionless time this means that the final time is $\hat{\tau}_f = 1$ and $\tau_{ref} = 0.08333\,s$. The follow reference values have used in BOCOP: $h_{1,ref} = 10^{-11}$, $h_{2,ref} = 10^{-2}$, $h_{3,ref} = 10^{-10}$ $h_{4,ref} = 10^{-10}$, $h_{5,ref} = 10^{-10}$, $h_{6,ref} = 10^{-12}$ while a the Midpoint method and tolerance $tol = 10^{-18}$ have been adopted.
Table 3 shows the maximum energy per 10 cycles for a constant value $\hat{R}_l = 0.004399$, which is much smaller than the resonance load resistance $\hat{R}_{l,resonance} = 4.399$, and different couples of values $\hat{L}_{l,min}$ and $\hat{L}_{l,max}$.

Table 3. Maximum energy per 10 cycles for a constant value $\hat{R}_l = 0.004399$ and different couples of values $\hat{L}_{l,min}$ and $\hat{L}_{l,max}$. $n_{steps} = 10000$.

$\hat{L}_{l,\min}$	$\hat{L}_{l,\max}$	Energy per 10 cycles (pJ)
1.0	1.0	0.1878
1.0	1.1	0.2168
1.0	1.2	0.2517
1	1.3	0.2820
0.9	1.0	0.2209
0.8	1.0	0.2709
0.7	1.0	0.3422

Table 2. Dimensionless notation, coefficients and equations for the load consisting of a resistor and a controllable inductance

Notation

$$\hat{\tau} \equiv \frac{\tau}{\tau_{ref}} \qquad \hat{L}_l \equiv \frac{L_l}{L_{l,ref}}$$

$$\hat{h}_1 \equiv \frac{z}{z_{ref}} \qquad \hat{h}_2 \equiv \frac{\dot{z}}{\dot{z}_{ref}} \qquad \hat{h}_3 \equiv \frac{q_t}{q_{t,ref}} \qquad \hat{h}_4 \equiv \frac{q_h}{q_{h,ref}} \qquad \hat{h}_5 \equiv \frac{\dot{q}_h}{\dot{q}_{h,ref}} \qquad \hat{h}_6 \equiv \frac{E}{E_{ref}}$$

Coefficients

$$A_{12} \equiv \frac{\dot{z}_{ref}\tau_{ref}}{z_{ref}}$$

$$A_{21} \equiv -\left(\omega_N^2 + \frac{\theta^2}{M_T C_p}\right)\frac{z_{ref}\tau_{ref}}{\dot{z}_{ref}} \qquad A_{22} \equiv -2\zeta_m \omega_N \tau_{ref} \qquad A_{23} \equiv -\frac{\theta}{M_T C_p}\frac{q_{t,ref}\tau_{ref}}{\dot{z}_{ref}} \qquad A_{2w} \equiv -\frac{a\tau_{ref}}{\dot{z}_{ref}} \qquad B_{2w} \equiv 2\pi f \tau_{ref}$$

$$A_{31} \equiv -\frac{\theta}{R_{hp}C_p}\frac{z_{ref}\tau_{ref}}{q_{t,ref}R_{hp}} \qquad A_{33} \equiv -\frac{\tau_{ref}}{R_{hp}C_p} \qquad A_{35} \equiv \frac{\dot{q}_{h,ref}\tau_{ref}}{q_{t,ref}}$$

$$A_{45} \equiv \frac{\dot{q}_{h,ref}\tau_{ref}}{q_{h,ref}}$$

$$A_{51} \equiv -\frac{\theta}{L_{l,ref}C_p}\frac{z_{ref}\tau_{ref}}{\dot{q}_{h,ref}} \qquad A_{53} \equiv -\frac{1}{L_{l,ref}C_p}\frac{q_{t,ref}\tau_{ref}}{\dot{q}_{h,ref}} \qquad A_{55} = -\frac{R_{hs}+R_l}{L_{l,ref}}\tau_{ref}$$

$$A_{65} \equiv R_l \frac{\dot{q}_{h,ref}^2 \tau_{ref}}{E_{ref}}$$

Equations

$$\frac{d\hat{h}_1}{d\hat{\tau}} = A_{12}\hat{h}_2$$

$$\frac{d\hat{h}_2}{d\hat{\tau}} = A_{21}\hat{h}_1 + A_{22}\hat{h}_2 + A_{23}\hat{h}_3 + A_{2w}\cos\left(B_{2w}\hat{\tau}\right)$$

$$\frac{d\hat{h}_3}{d\hat{\tau}} = A_{31}\hat{h}_1 + A_{33}\hat{h}_3 + A_{35}\hat{h}_5$$

$$\frac{d\hat{h}_4}{d\hat{\tau}} = A_{45}\hat{h}_5$$

$$\frac{d\hat{h}_5}{d\hat{\tau}} = \frac{1}{\hat{L}}\left(A_{51}\hat{h}_1 + A_{53}\hat{h}_3 + A_{55}\hat{h}_5\right)$$

$$\frac{d\hat{h}_6}{d\hat{\tau}} = A_{65}\hat{h}_5^2$$

Initial conditions

$$\hat{h}_i\left(\hat{\tau} = 0\right) = 0 \quad \left(i = 1{,}6\right)$$

The optimal control provides a larger amount of harvested energy than using a constant value $\hat{L}=1.0$ of the inductance. The maximum harvested energy increases by increasing the width of the interval $\left[\hat{L}_{l,min},\hat{L}_{l,max}\right]$, this interval being placed below or above the value $\hat{L}=1.0$. Therefore, the control $\hat{L}_l$ is of the bang-bang-type. This is clearly shown in Fig. 1 (a),(c),(e),(g),(i),(k). The harvested energy increases rapidly in the first cycle and has a much slower increase in the next nine cycles – see Fig. 1(b),(d),(f),(h),(j), (l). The relative energy gain in the first cycle is larger at larger widths of the interval of variation of the controllable inductance.

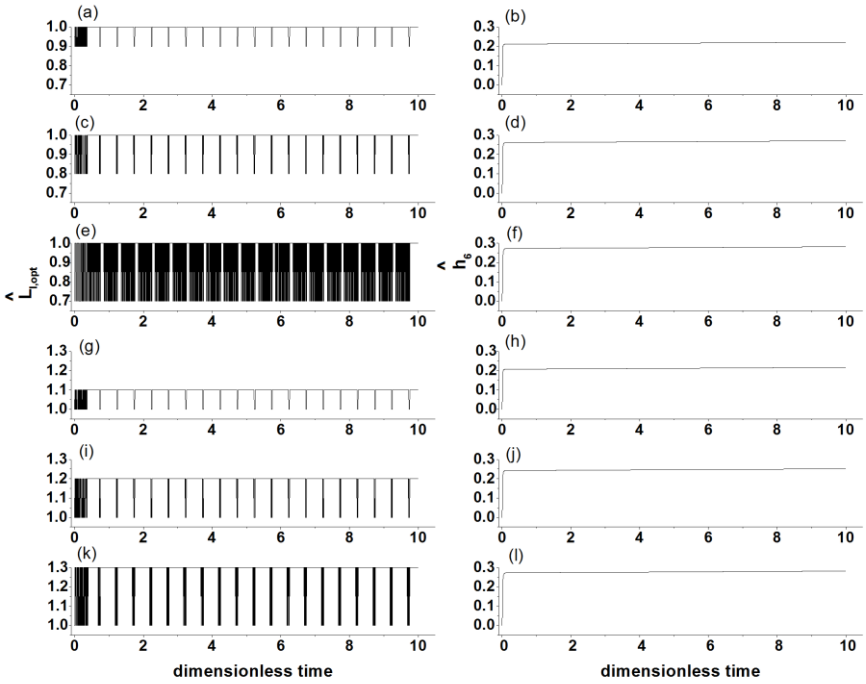

Fig. 1. Dimensionless optimal control $\hat{L}_{l,opt}$ (left column) and dimensionless maximum harvested energy $\hat{h}_6$ (right column) as a function of dimensionless time $\hat{\tau}$. (a,b) - $\hat{L}_{l,min}=0.9$, $\hat{L}_{l,max}=1.0$; (c,d) - $\hat{L}_{l,min}=0.8$, $\hat{L}_{l,max}=1.0$; (e,f) $\hat{L}_{l,min}=0.7$, $\hat{L}_{l,max}=1.0$; (g,h) $\hat{L}_{l,min}=1.0$, $\hat{L}_{l,max}=1.1$; (i,j) $\hat{L}_{l,min}=1.0$, $\hat{L}_{l,max}=1.2$; (k,l) $\hat{L}_{l,min}=1.0$, $\hat{L}_{l,max}=1.3$; Ten cycles are considered ($\hat{\tau}_f=10$ and $\tau_{ref}=0.008333\,s$) and $n_{steps}=15000$. $\hat{R}_l=0.004399$.

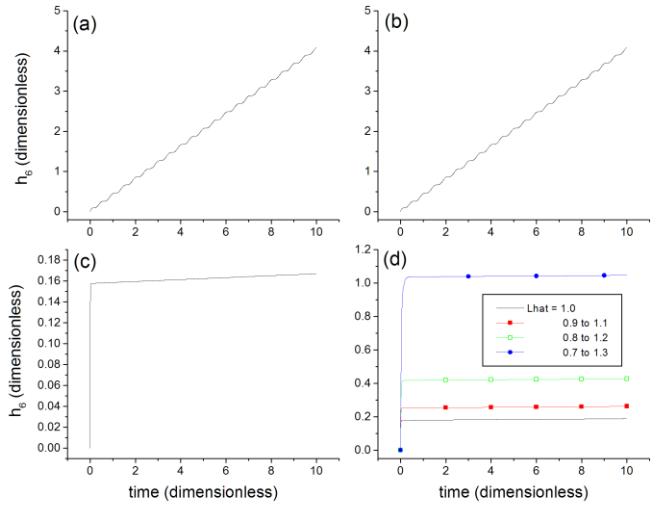

Fig. 2. Dimensionless harvested energy $\hat{h}_6$ as a function of the dimensionless time $\hat{\tau}$. (a) Resonance load resistance $\hat{R}_l = 4.399$ and $\hat{L}_{ref} = 0.01$. Optimal control with variable inductance ranging between $\hat{L}_{l,min} = 0.7\hat{L}_{ref}$ and $\hat{L}_{l,max} = 1.3\hat{L}_{ref}$. (b) As (a) for $\hat{L}_{ref} = 1.0$. (c) as (a) for $\hat{R}_l = 0.004399$; $\left[\hat{L}_{l,min}, \hat{L}_{l,max}\right]$ = $\left[\hat{L}_{ref}, \hat{L}_{ref}\right]$, $\left[0.9\hat{L}_{ref}, 1.1\hat{L}_{ref}\right]$, $\left[0.8\hat{L}_{ref}, 1.2\hat{L}_{ref}\right]$ and $\left[0.7\hat{L}_{ref}, 1.3\hat{L}_{ref}\right]$ $\left[0.9\hat{L}_{ref}, 1.1\hat{L}_{ref}\right]$ (d) As (c) for $\hat{R}_l = 0.004399$, $\hat{L}_{ref} = 1.0$. Ten cycles are considered ($\hat{\tau}_f = 10$ and $\tau_{ref} = 0.008333\,s$) and $n_{steps} = 15000$.

The time variation of the harvested energy significantly depends on the value of the load resistance $\hat{R}_l$. In case $\hat{R}_l$ equals the resonance value 4.399, the harvested energy increases linearly in time for small values of the controllable inductance $\hat{L}_l$ (Fig. 2(a)) as well for large values of $\hat{L}_l$ (Fig. 2(b)). When a smaller value of the load resistance is considered ($\hat{R}_l = 0.004399$), most energy is harvested in the first cycle while the next cycles contribute a small amount of energy (Figs. 2(c) and 2(d)). The energy harvested in the first cycle is smaller for small values of the controllable inductance $\hat{L}_l$ than for larger values of $\hat{L}_l$ (compare Fig. 2(c) and Fig. 2(d)). At small values of $\hat{L}_l$, the optimal control provides almost the same amount of harvested energy as a constant value of $\hat{L}_l$ (Fig. 2(c)). At large values of $\hat{L}_l$, the

energy harvested in the first cycle by using an optimal control strategy increases by increasing the width of the interval $\left[\hat{L}_{l,min},\hat{L}_{l,max}\right]$ (Fig. 2(d)).

Table 4. Energy per ten cycles for different values of the load resistance $\hat{R}_l$ and several intervals of variation $\left[\hat{L}_{l,min},\hat{L}_{l,max}\right]$ of the controllable inductance $\hat{L}_l$.

$\hat{R}_l$	$\hat{L}_{ref}$	$\hat{L}_{l,min}/\hat{L}_{ref}$	$\hat{L}_{l,max}/\hat{L}_{ref}$	Energy per 10 cycles (pJ)
		1	1	4.091280
	10^{-2}	0.9	1.1	4.091280
		0.8	1.2	4.091280
4.399		0.7	1.3	4.091281
		1	1	4.091370
	1	0.9	1.1	4.091410
		0.8	1.2	4.091451
		0.7	1.3	4.091492
		1	1	0.165884
	10^{-2}	0.9	1.1	0.166241
		0.8	1.2	0.166601
0.004399		0.7	1.3	0.166954
		1	1	0.188354
	1	0.9	1.1	0.262189
		0.8	1.2	0.427042
		0.7	1.3	1.046151

Detailed results for the harvested energy per ten cycles are provided in Table 4. In case the load resistance $\hat{R}_l$ equals the resonance value 4.399, the load inductance $\hat{L}_l$ is not recommended to be used as a control since the harvested energy does not depend of the interval of variation $\left[\hat{L}_{l,min},\hat{L}_{l,max}\right]$ (for the values used in this study). When smaller values of the load resistance are considered, $\hat{L}_l$ may be used as a control, provided the width of its interval of variation is large enough.

4 Energy storage in capacitor

In this section the harvested electrical energy is stored in a capacitor. This approach has been treated in several papers, where capacitors with constant or variable capacitance have been considered (see [7] for instance). Using a variable capacitive load can be used to match the frequency of the external vibration in real time (see [6] for discussions). The power may be maximized by placing a dc-dc converter

between the rectifier and the storage cells [7]. A classical H-bridge switching drives is placed at the interface between several transducers excited by a white noise with a global energy storage bus has been proposed in [8], where the drive current vector is controlled by rapid alternation of the four switches, with the objective to maximize the harvested power. Transistor-based rectifiers were also treated in literature [9]. The effects of different technology capacitors on energy harvester performance have been treated in a commercial context in [10]. The power consumption by the controller and the leakage current have been considered. Other authors assumed the energy is stored in a battery [11]. In that case, the harvesting circuits consist of a full-bridge rectifier and a switching DC-DC step-down converter. At low level excitation the rectifier charges the battery while at high level excitation the battery runs the DC-DC converter which delivers four times more power to the battery than through direct charging from rectifier. An harmonic excitation has been assumed at the resonance frequency of the transducer and the design of the electronic control system was based on the idea of impedance matching.

Three type of energy harvesting circuits are commonly in usage [2]: (i) the passive diode-rectifier circuit (which is the simplest but has lower efficiency), (ii) the semi-active circuit (where the output voltage may be processed to increase its magnitude and change its phase in order to maximize the output power) and (iii) the active circuit (where appropriate electrical boundary conditions are applied to the piezoelectric element to maximize the effectiveness of the harvester). A passive diode-rectifier circuit is assumed here.

Notice that the characteristic time of the charging process of the capacitor should normally be larger that any other characteristic time of the energy harvesting system [12]. Also, the discharging of the capacitor by the user should start before the capacitor is fully charged.

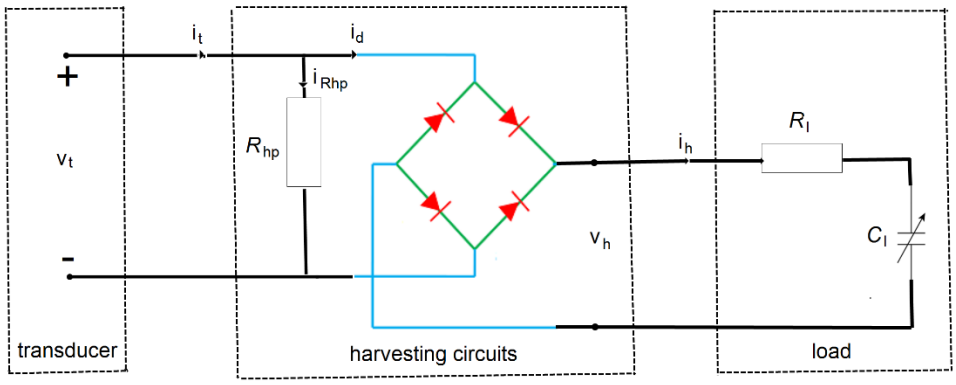

Fig. 3. The system considered here. Harvesting circuit consists of a parallel resistor of resistance R_{hp} and a rectifier bridge. The electric load consists of a capacitor of controllable capacitance C_l and a series resistance R_l.

Figure 3 shows the system considered here. The harvesting circuits consist of a parallel resistor of resistance R_{hp} , a rectifier bridge and the electric load whose main components are a capacitor of capacitance C_l and a series resistance R_l. The power losses in the electronic circuit are assumed quadratic and purely resistive [13]. The electric currents at the inlet and outlet of the bridge are denoted i_d and i_h, respectively.

The voltage at bridge inlet equals the voltage v_t provided by the transducer while the voltage at bridge outlet is denoted v_h. An ideal rectifier bridge is considered here. Therefore:

$$v_h = |v_t| \tag{9}$$

and the power conservation across the bridge gives:

$$i_d v_t = i_h v_h \tag{10}$$

Notice that i_d and i_h represent the time variation of the electric charges q_d and q_h entering and exiting the bridge, respectively, i.e.

$$i_d = \dot{q}_d \tag{11}$$

$$i_h = \dot{q}_h \tag{12}$$

Notice that $\dot{q}_h$ is also the time variation of the capacitor charge. From Eqs. (9),(10),(11) and (12) one finds:

$$\dot{q}_d = sign(v_t)\dot{q}_h = sign\left(-\frac{q_t + \theta z}{C_p}\right)\dot{q}_h \tag{13a,b}$$

where $sign(v_t)$ denotes the sign of v_t (or, in other words, $|v_t|/v_t$) and Eq. (14) of paper [1] has been considered. A relationship similar with Eq. (13a) has been used in [13]. The Kirchoff's law for nodes states:

$$i_t = i_{Rhp} + i_d \tag{14}$$

Usage of Eqs. (14),(11),(13b) and Eq. (14) of paper [1] gives:

$$\dot{q}_t = -\frac{q_t + \theta z}{C_p R_{hp}} + sign\left(-\frac{q_t + \theta z}{C_p}\right)\dot{q}_h \tag{15}$$

The current i_h vanished when the voltage v_h at bridge outlet is lower than the voltage $v_{C_l} = q_h / C_l$ across the capacitor. Therefore, the charging of the capacitor is not necessary a continuous process. This has been already observed [14]. Taking into account Eq. (11) and the Ohm law, one sees that:

$$\dot{q}_h = \begin{cases} \dfrac{1}{R_l}\left[\left|-\dfrac{q_t+\theta z}{C_p}\right|-\dfrac{q_h}{C_l}\right] & \text{if} \quad \left|-\dfrac{q_t+\theta z}{C_p}\right| > \dfrac{q_h}{C_l} \\ 0 \quad \text{otherwise} \end{cases} \tag{16}$$

The term in the right parentheses in the r.h.s. of Eq. (16) represents the voltage difference between the harvesting circuits and the capacitor. When this difference is positive the electric charge is flowing towards the capacitor. The Eq. (16) is similar with Eq. (2.3b) of [12].

Equation (6) of paper [3], and Eqs. (15) and (16) constitute a system of three equations with three unknown, i.e. z, q_t and q_h. These equations are solved by using the initial conditions Eqs. (8) and (9) of paper [3] and Eq. (6), respectively. Notice that the initial condition Eq. (6) means that the capacitor is not charged at $\tau = 0$.

The electric energy $E_{C_l,T}$ stored in the capacitor during the time interval T is:

$$E_{C_l,T} = \int_0^T \frac{q_h}{C_l}\dot{q}_h d\tau \tag{17}$$

Equation (1) has been used in Eq. (17). The first term in the kernel of the integral in Eq. (17) is the voltage v_{C_l} across the capacitor while the second term is the current entering the condenser, as described by Eq. (12). The objective is to maximize the electric energy $E_{C_l,T}$ by using a time variable capacitance C_l, which is used as a control. Notice that the cost function is defined in [15] as the power extracted by the transducer minus the transmission losses. Negligible losses are assumed here and this hypothesis has been checked later.

To prepare the Mayer problem we define the new dependent variable E_{C_l} by using the equation:

$$\frac{dE_{C_l}}{d\tau} = \frac{q_h}{C_l}\dot{q}_h \tag{18}$$

which is to be solved by using the initial condition Eq. (12) of paper [3]. The objective is defined by Eq. (13) of paper [3].

Table 5 shows the dimensionless notation, the coefficients and the equations for a system where the load consists of a resistor and a controllable capacitance.

Table 5. Dimensionless notation, coefficients and equations for the load consisting of a resistor and a controllable capacitance.

Notation

$$\hat{\tau} \equiv \frac{\tau}{\tau_{ref}} \qquad \hat{C}_l \equiv \frac{C_l}{C_{l,ref}}$$

$$\hat{h}_1 \equiv \frac{z}{z_{ref}} \qquad \hat{h}_2 \equiv \frac{\dot{z}}{\dot{z}_{ref}} \qquad \hat{h}_3 \equiv \frac{q_t}{q_{t,ref}} \qquad \hat{h}_4 \equiv \frac{q_h}{q_{h,ref}} \qquad \hat{h}_5 \equiv \frac{E_{C_l}}{E_{ref}}$$

Coefficients

$$A_{12} \equiv \frac{\dot{z}_{ref}\tau_{ref}}{z_{ref}}$$

$$A_{21} \equiv -\left(\omega_N^2 + \frac{\theta^2}{M_T C_p}\right)\frac{z_{ref}\tau_{ref}}{\dot{z}_{ref}} \qquad A_{22} \equiv -2\zeta_m\omega_N\tau_{ref} \qquad A_{23} \equiv -\frac{\theta}{M_T C_p}\frac{q_{t,ref}\tau_{ref}}{\dot{z}_{ref}} \qquad A_{2w} \equiv -\frac{a\tau_{ref}}{\dot{z}_{ref}} \qquad B_{2w} \equiv 2\pi f\tau_{ref}$$

$$D_1 \equiv -\frac{\theta z_{ref}}{C_p} \qquad D_3 \equiv -\frac{q_{t,ref}}{C_p} \qquad D_4 \equiv \frac{q_{h,ref}}{C_{l,ref}}$$

$$A_{31} \equiv \frac{1}{R_{hp}}\frac{\tau_{ref}}{q_{t,ref}} \qquad A_{32} \equiv \frac{\tau_{ref}}{R_l q_{t,ref}}$$

$$A_{41} \equiv \frac{1}{R_l}\frac{\tau_{ref}}{q_{h,ref}}$$

$$A_{51} \equiv \frac{1}{R_l}\frac{\tau_{ref}}{E_{ref}}$$

Equations

$$\frac{d\hat{h}_1}{d\hat{\tau}} = A_{12}\hat{h}_2$$

$$\frac{d\hat{h}_2}{d\hat{\tau}} = A_{21}\hat{h}_1 + A_{22}\hat{h}_2 + A_{23}\hat{h}_3 + A_{2w}\cos\left(B_{2w}\hat{\tau}\right)$$

$$\frac{d\hat{h}_3}{d\hat{\tau}} = \begin{cases} A_{31}\left(D_1\hat{h}_1 + D_3\hat{h}_3\right) + A_{32}sign\left(D_1\hat{h}_1 + D_3\hat{h}_3\right)\left(\left|D_1\hat{h}_1 + D_3\hat{h}_3\right| - D_4\dfrac{\hat{h}_4}{\hat{C}_l}\right) & \text{if} \quad \left|D_1\hat{h}_1 + D_3\hat{h}_3\right| - D_4\dfrac{\hat{h}_4}{\hat{C}_l} > 0 \\ A_{31}\left(D_1\hat{h}_1 + D_3\hat{h}_3\right) & \text{otherwise} \end{cases}$$

$$\frac{d\hat{h}_4}{d\hat{\tau}} = \begin{cases} A_{41}\left(\left|D_1\hat{h}_1 + D_3\hat{h}_3\right| - D_4\dfrac{\hat{h}_4}{\hat{C}_l}\right) & \text{if} \quad \left|D_1\hat{h}_1 + D_3\hat{h}_3\right| - D_4\dfrac{\hat{h}_4}{\hat{C}_l} > 0 \\ 0 & \text{otherwise} \end{cases}$$

$$\frac{d\hat{h}_5}{d\hat{\tau}} = \begin{cases} A_{51}D_4\dfrac{\hat{h}_4}{\hat{C}_l}\left(\left|D_1\hat{h}_1 + D_3\hat{h}_3\right| - D_4\dfrac{\hat{h}_4}{\hat{C}_l}\right) & \text{if} \quad \left|D_1\hat{h}_1 + D_3\hat{h}_3\right| - D_4\dfrac{\hat{h}_4}{\hat{C}_l} > 0 \\ 0 & \text{otherwise} \end{cases}$$

Initial conditions

$$\hat{h}_i\left(\hat{\tau} = 0\right) = 0 \quad \left(i = 1,5\right)$$

4.1 Results

We have performed several tests in order to find the most suitable number of steps n_{steps} to divide the interval $\lfloor 0, \hat{\tau}_f \rfloor$. A constant value have been adopted for the control $\hat{C}_l$. The results obtained by using DDRIV3 solver are used as a reference. Table 6 shows results obtained by using two BOCOP algorithms (Midpoint and Gauss) and DDRIV3 solver as a function of the number of steps n_{steps} for two constant values of the dimensionless load capacitance $\hat{C}_l$. The Gauss algorithm needs smaller number of steps to obtain to provide results close to those provided by the reference solver DDRIV3. However, the computing time is very long in this case. The algorithm Midpoint and the value $n_{steps} = 40000$ are adopted for next computations, as a compromise between better results accuracy and shorter computing time.

Table 6. Dependence of accuracy on the number of steps for DDRIV3 solver and two BOCOP algorithms. Two constant values of $\hat{C}_l$ have been considered.

Constant value of $\hat{C}_l$		1000			100	
Solver	DDRIV3 (reference)	BOCOP		DDRIV3 (reference)	BOCOP	
Algorithms		Midpoint	Gauss		Midpoint	Gauss
Number of steps						
1000	**0.1560**	1.4285	0.6784	**1.5627**	18.4094	7.1500
2000	**0.1552**	0.5877	0.3131	**1.5540**	6.1196	3.1600
3000	**0.1553**	0.3826	0.2242	**1.5561**	3.8831	2.2500
4000	**0.1551**	0.2966	0.1898	**1.5532**	3.0009	1.9030
5000	**0.1552**	0.2526	0.1739	**1.5540**	2.5428	1.7400
6000	**0.1552**	0.2266	0.1659	**1.5546**	2.2745	1.6600
7000	**0.1551**	0.2098	0.1616	**1.5532**	2.1055	1.6100
8000	**0.1550**	0.2016	0.1543	**1.5525**	2.0235	1.5960
9000	**0.1550**	0.1901	0.1567	**1.5521**	1.9061	1.5737
10000	**0.1551**	0.1840	0.1569	**1.5531**	1.8448	1.5724
15000	**0.1550**	0.1685		**1.5518**	1.6877	
20000	**0.1550**	0.1629		**1.5516**	1.6319	
25000	**0.1549**	0.1606		**1.5515**	1.6090	
30000	**0.1549**	0.1586		**1.5514**	1.5883	
35000	**0.1549**	0.1576		**1.5515**	1.5789	
40000	**0.1549**	0.1570		**1.5515**	1.5719	
45000	**0.1549**			**1.5514**		
50000	**0.1549**			**1.5515**		

Several optimal control tests have been performed with the controllable capacitance $\hat{C}_l$ ranging between different values $\hat{C}_{l,\min}$ and $\hat{C}_{l,\max}$. These tests showed that the optimal capacitance consists of a constant value $\hat{C}_{l,opt} = \hat{C}_{l,\min}$. There is a simple explanation for this result: when the capacitance has a smaller value, the voltage across the capacitor is larger and therefore a larger amount of energy is stored (see Eq. (17)).

Results are shown next for two cases, namely a capacitor with a larger and a smaller capacitance, respectively. Since the optimal capacitance is a constant, here we present results obtained with the solver DDRIV3 for $n_{steps} = 50000$. Ten cycles were analyzed. In terms of the dimensionless time this means that the final time is $\hat{\tau}_f = 1$ and $\tau_{ref} = 0.08333\, s$. The follow reference values have used: $h_{1,ref} = 10^{-10}$, $h_{2,ref} = 1$, $h_{3,ref} = 10^{-7}$, $h_{4,ref} = 10^{-5}$, $h_{5,ref} = 10^{-9}$ while $C_{l,ref} = 10^{-6}$ and $R_l = 1000\,\Omega$.

Figures 4 and 5 show results for a capacitor with a large optimal capacitance, i.e. $\hat{C}_{l,opt} = 1000.$ The optimal time variation of the main quantities in the first cycle is obviously different than in the next cycles (compare Fig. 4 and Fig. 5).

First, let us look to the first cycle (Fig. 4) The electric charge q_t in the piezoelectric element has a time variation similar with that of the deformation z_t, as expected. The larger the deformation z_t is, the larger the electric charge in the piezoelectric element is. The deformation z_t and the vibration speed $\dot{z}_t$ have a strong variation in the beginning of cycle. This induces a similar time variation for the voltage across the piezoelectric element v_t and the electric current i_d entering the rectifying bridge, followed by the voltage across the load v_h and the current entering the load i_h. Toward the end of the first cycle these currents and voltages seem to become constant (see Fig. 4(f),(g),(h),(i)). In fact, they have a sinusoidal time variation of a much smaller amplitude, which is clearly visible in the cycles two to ten (see Fig. 5 (f),(g),(h),(i)). The electric charge q_h and the voltage across the condenser v_{C_l} have a strong time variation in the beginning of the first cycle, followed by a smaller increase (Fig. 4(d) and Fig. 4(j), respectively). Therefore, the energy accumulated in the condenser E_{C_l} has a similar time variation (Fig. 4(e)).

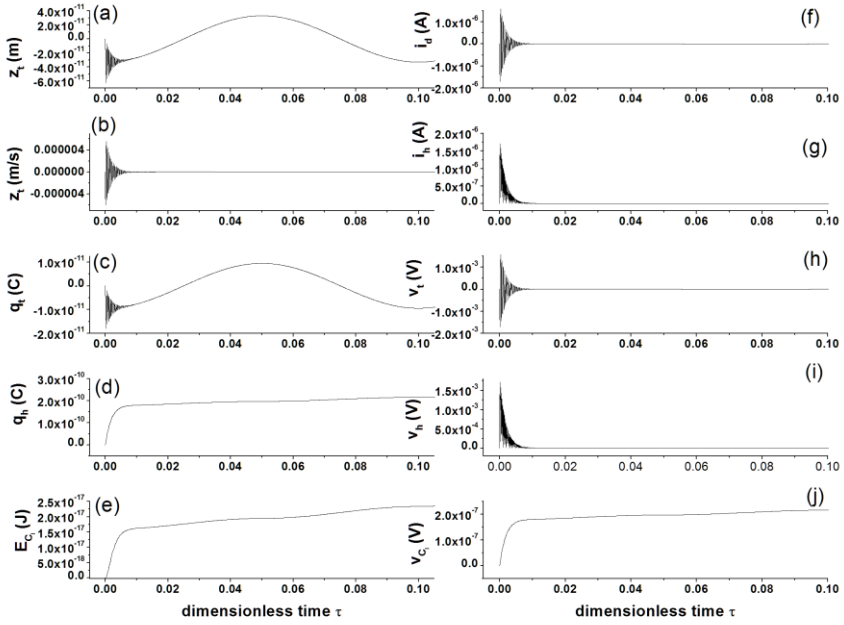

Fig. 4. Several quantities as functions of the dimensionless time $\hat{\tau}$ during the first of the ten cycles for an optimal capacitance $\hat{C}_{l,opt} = 1000.$ (a) displacement z_t; (b) speed $\dot{z}_t$; (c) piezoelectric charge q_t; (d) electric charge stored in the load capacitor q_h; (e) energy stored in the load capacitor E_{C_l}; (f) electric current entering the rectifier bridge i_d; (g) electric current entering the load i_h; (h) voltage across the piezoelectric element v_t; (i) voltage across the load v_h; (j) voltage across the capacitor v_{C_l}.

Next, let us look to the cycles two to ten (Fig. 5). Most quantities have a periodic variation of smaller amplitudes as compared with those of Fig. 4. The rectifying process by the bridge is clearly seen in the variation of i_h and v_h (Fig. 5(g) and Fig. 5(i), respectively). The charge q_h and the voltage across the capacitor v_{C_l} increase linearly (Fig. 5(d) and 5(j), respectively) and they have larger values than at the end of the first cycle, as expected (compare with Fig. 4(d) and 4(j), respectively). Also, the energy accumulated in the capacitor increases slightly non-linearly in time (Fig. 5(e)).

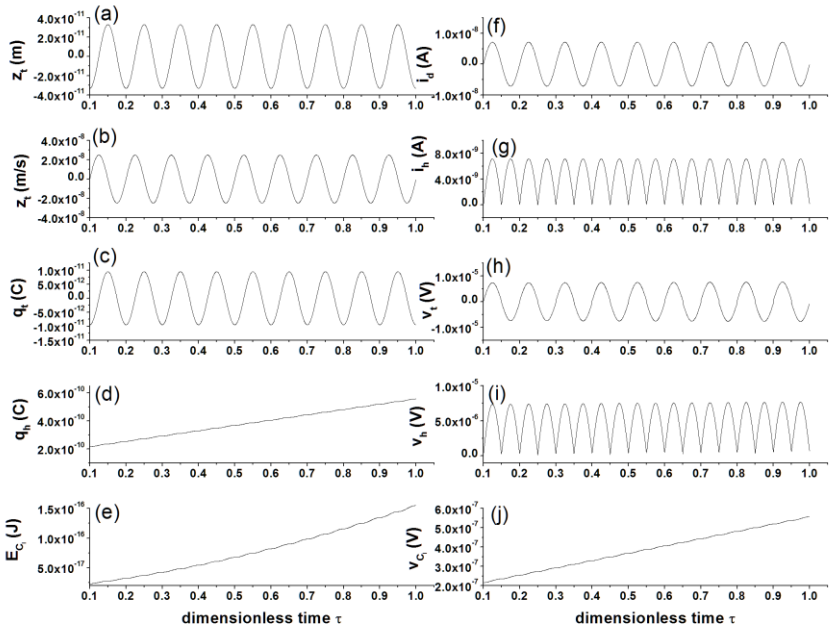

Fig. 5 As Fig. 4 for the cycles two to ten.

Figures 6 and 7 show results for a capacitor with a smaller optimal capacitance, i.e. $\hat{C}_{l,opt}=100.$ Figure 6 refers to the first cycle. For most quantities the results are similar with those of Fig. 4 for the larger capacitance $\hat{C}_{l,opt}=1000.$ However, the voltage across the capacitor v_{C_l} and the energy accumulated in the capacitor E_{C_l} are obviously larger in case of $\hat{C}_{l,opt}=100$ than in case of $\hat{C}_{l,opt}=1000$ (compare Fig. 6(j) and (e), on one hand with Fig. 4(j) and (i), of the other hand). This is the result of the smaller capacitance in the first case, as already explained.

Figure 7 refers to the cycles two to ten. The time variation of most quantities is similar with that of Fig. 5 for the larger capacitance $\hat{C}_{l,opt}=1000.$ The values of the voltage across the load v_h, the voltage across the capacitor v_{C_l} and the energy accumulated in the capacitor E_{C_l} are obviously larger in case of $\hat{C}_{l,opt}=100$ than in case of $\hat{C}_{l,opt}=1000$ (compare Fig. 7(i), (j) and (e), on one hand with Fig. 5(i), (j) and (i), of the other hand). This is the result of a smaller capacity in the first case.

These results show that a smaller load capacitance is to be recommended. However, such a smaller capacitance is able to store a limited amount of energy and this puts some limitation on the number of cycles harvested before the load capacitor is to be discharged by the user. Notice that in our calculations the capacitor has not been fully charged after ten cycles.

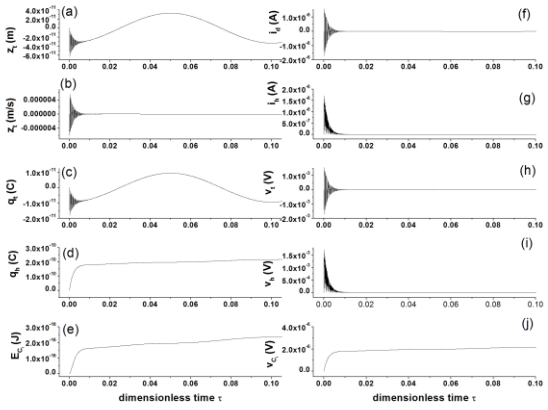

Fig. 6. As Fig. 4 for an optimal capacitance $\hat{C}_{l,opt} = 100.$

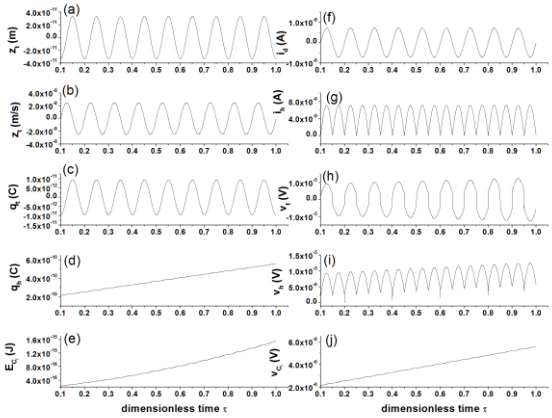

Fig. 7. As Fig. 5 for an optimal capacitance $\hat{C}_{l,opt} = 100.$

5.Conclusions

When the load consists of a resistor and a controllable inductance, the maximum harvested energy depends on the value of the load resistance $\hat{R}_l$. If it equals the

resonance value, the harvested energy increases linearly in time for all values of the controllable inductance $\hat{L}_l$. If $\hat{R}_l$ is much smaller than the resonance value, most energy is harvested in the first cycle while the next cycles contribute a small amount of energy. The energy harvested in the first cycle is smaller for smaller values of $\hat{L}_l$. At large values of $\hat{L}_l$, the energy harvested in the first cycle by using an optimal control strategy increases by increasing the width of the interval $\left[\hat{L}_{l,min},\hat{L}_{l,max}\right]$ of inductance variation. When ten cycles are considered, $\hat{L}_l$ may be used as a control only for a load resistance $\hat{R}_l$ smaller than the resonance value, provided the interval $\left[\hat{L}_{l,min},\hat{L}_{l,max}\right]$ is large enough. If $\hat{R}_l$ equals the resonance value, the harvested energy does not depend of the width of that interval. Therefore, $\hat{L}_l$ is not recommended to be used as a control.

When the electric load consists of a capacitor of controllable capacitance C_l and a series resistance R_l, the energy harvested in the first cycle is larger than that harvested in any of the next cycles. The optimal capacitance value is constant and equals the smallest allowed value. But the capacitance should be large enough to store the energy needed by the user during a limited number of cycles of the vibratory energy sources.

The following conclusions cover all the particular cases treated in this paper. First, the maximum harvesting performance is obtained when the control parameters are constant or have a bang-bang-type time evolution. Second, sizing the load is strongly constrained by the characteristics of the vibratory energy sources. Third, the number of cycles used for optimization is an important design parameter, especially in case of storing energy in capacitors. Fourth, the most suitable applications are those which may be powered by using the energy harvested from a single cycle.

References

[1] Badescu V., *Best operation strategies for piezoelectric vibration energy harvesters.* I. *Theory*, J. Eng. Sci. and Innovation, **8**, 2, 2023, p. 171-186.

[2] Zhang L., Zheng G., Li J., *Adaptive active piezoelectric energy harvester*, Int. J. of Digital Content Technology and its applications, **6**, 2012, p. 410- 419.

[3] Badescu V., *Best operation strategies for piezoelectric vibration energy harvesters.* II. *Application to simple or induction-assisted resistive loads*, J. Eng. Sci. and Innovation, **8**, 3, 2023, p. 251-268.

[4]. Du Toit N.E., *Modeling and design of a MEMS piezoelectric vibration energy harvester*, MsD thesis, MIT, May 2005.

[5] Stephen N.G., *On the energy harvesting from ambient vibration*, J Sound and Vibration, **293**, 2006, p. 409-425.